

Replenish and Relax: Explaining Logarithmic Annealing in Ion-Implanted *c*-Si

Laurent Karim Béland,^{*} Yonathan Anahory,[†] Dries Smeets, Matthieu Guihard, Peter Brommer,[‡] Jean-François Joly,[§]
Jean-Christophe Pothier,^{||} Laurent J. Lewis,[¶] Normand Mousseau,^{**} and François Schiettekatte^{††}

*Regroupement Québécois sur les Matériaux de Pointe (RQMP), Département de physique, Université de Montréal,
Case Postale 6128, Succursale Centre-ville, Montréal, Québec, H3C 3J7, Canada*

(Received 10 April 2013; published 4 September 2013)

We study ion-damaged crystalline silicon by combining nanocalorimetric experiments with an off-lattice kinetic Monte Carlo simulation to identify the atomistic mechanisms responsible for the structural relaxation over long time scales. We relate the logarithmic relaxation, observed in a number of disordered systems, with heat-release measurements. The microscopic mechanism associated with this logarithmic relaxation can be described as a two-step replenish and relax process. As the system relaxes, it reaches deeper energy states with logarithmically growing barriers that need to be unlocked to replenish the heat-releasing events leading to lower-energy configurations.

DOI: [10.1103/PhysRevLett.111.105502](https://doi.org/10.1103/PhysRevLett.111.105502)

PACS numbers: 81.40.Ef, 07.20.Fw, 61.43.Bn, 61.72.Cc

Fatigue and aging of materials are, in large part, determined by the evolution of the atomic-scale structure in response to strains and perturbations. The coupling between microscopic structure and long time scales remains one of the main challenges in materials study. This problem affects materials ranging from somewhat simple crystalline systems to glasses, alloys, and cements, and is at the root of phenomena affecting materials reliability, aging, and fatigue. Over the years, their evolution has been characterized by various models based on continuous, mesoscopic, or atomic-scale models and generally fitted to experimental data [1–10]. Direct comparison between models, experiments, and atomic-scale simulations, however, has been limited because of the often extensive time scale difference between the three, leaving considerable space for interpretation in the fitting procedure even when describing apparently simple relaxation processes such as logarithmic relaxation observed in polymer glasses, for example [11–13], and in ion-implanted amorphous and crystalline systems [14–16]. Here, we select ion implantation-induced disorder in monocrystalline silicon (*c*-Si), a controlled approach for perturbing samples that can be closely reproduced numerically [17,18]. Combined with calorimetric measurements, ion implantation is an ideal technique for studying the kinetics and thermodynamics of complex structures evolution in a systematic way.

Many models have been proposed for describing the accumulation and annealing of ion-induced disorder in materials. The Frenkel pair model, for example, describes the disorder in terms of isolated vacancies (*V*) and interstitials (*I*) [19]; in contrast, MD simulations show that the majority of defects induced by the impact of a single ion of a few keV are found in the form of heavily damaged zones commonly called amorphous pockets (APs) [17,20–22] that anneal in steps, with a wide range of activation energies that depend on the details of each APs' interface with

the crystal [17], as observed experimentally [23]. A popular model to account for damage accumulation proposed by Marqués and co-workers [24] describes APs as an assembly of *bound defects* corresponding to *IV* pairs [25]. While never detected directly in experiments, this mechanism was observed in various forms in short-time simulations [26–28]. As shown below, this model does not describe nanocalorimetry (NC) measurements correctly, and we are still seeking the correct atomic-scale relaxation model for implanted semiconductors.

In this Letter, we develop such a model by coupling the NC measurements of the annealing of low-energy, low-fluence implantation-induced disorder in *c*-Si with results from simulations performed using the recently proposed kinetic activation-relaxation technique (k-ART). k-ART is an off-lattice, self-learning kinetic Monte Carlo (KMC) algorithm [29,30] that makes it possible to follow the time evolution of large implanted simulation boxes over a time scale of up to a second or more, taking into account the full complexity of activated events and their associated long-range elastic effects over time scales comparable to the experiments. Results show that the broad, featureless heat release as a function of temperature measured by NC over several hundreds of kelvin is well reproduced by the k-ART simulations. Analysis of the atomistic simulations allows us to understand the microscopic origin of this logarithmic relaxation.

NC measures heat release or absorption as a function of temperature in thermodynamic and kinetic processes occurring at the nanoscale. The technique, described in Refs. [31,32], has been used to investigate phenomena ranging from melting point depression in nanoparticles [33] to disorder annealing in amorphous Si (*a*-Si) [14] and polycrystalline Si (poly-Si) [34]. The device consists of a low-stress, 250 nm thick SiN_x membrane supported by a 300 μm thick silicon frame. On top of the membrane, a Pt strip is used to measure the temperature and heat the

samples. The new device used here [35] features, underneath the membrane, a 330 nm thick *c*-Si strip, aligned with the heating strip. Heating rates reaching 10^5 K/s convert small amounts of heat released during disorder annealing into measurable power.

For these experiments, the samples and reference nanocalorimeters were in contact with a sample holder either maintained at room temperature (RT) or cooled with liquid nitrogen (LN). In the latter case, the membrane, surrounded by a thermal shield, reached 110 K. The silicon layer was implanted with Si^- at a fluence of 0.02–0.1 Si/nm^2 and an energy ranging from 10 to 100 keV produced by a negative sputter ion source. The current was measured and integrated with systematic error $<20\%$, although the relative uncertainty between different experiments within a series of implantations is much smaller. A slit was placed in front of the nanocalorimeter in order to implant the *c*-Si strip without damaging the SiN_x membrane on each side. The implanted area being $0.05 \times 0.55 \text{ cm}^2$, $(55\text{--}270) \times 10^9$ ions were implanted in each experiment. This corresponds to 0.1 ions per square nanometer. At such low fluence, there should be a very small proportion of collision cascade overlapping, so the experiments are comparable to simulations of single ion implantations. A delay of the order of 30 s occurred between the end of the implantation and the NC temperature scan, which lasts 10 ms. Heat release is measured during the first temperature scan. Subsequent scans are used as baseline experiments to account for the fact that the implanted and reference NCs are not identical [31,32].

Figure 1 shows as solid lines the heat release per unit temperature, dQ/dT , as a function of temperature, for different implantations. The amount of heat released is divided by the number of implanted ions. In order to compare with simulations below, results are scaled to 3 keV; i.e., they are multiplied by a ratio of 3 keV divided by the implantation energy. The data collected for 10 keV, 0.02 Si/nm^2 implants featured a raw amplitude of less than 7 nJ/K above 500 K, a region where the signal becomes dominated by the thermal losses, therefore featuring significant noise, so a smoothed curve is presented. For implantations at LN, there is a rapid increase near 200 K, followed by a slow, featureless decrease spanning several hundred degrees. Heat releases at similar amplitudes are observed for RT implants, but starting above 400 K. At higher fluences, the signal becomes flat (not shown) instead of slowly decreasing [36], a behavior observed in poly-Si [34] and *a*-Si [14].

These measurements suggest that the disorder consists of structures complex enough that no single activation energy can be associated with their annealing. Indeed, similar experiments involving H implantation, where discrete processes occur, do show distinct peaks, associated with vacancy mobility, on top of a broad background signal, related to more complex processes [36].

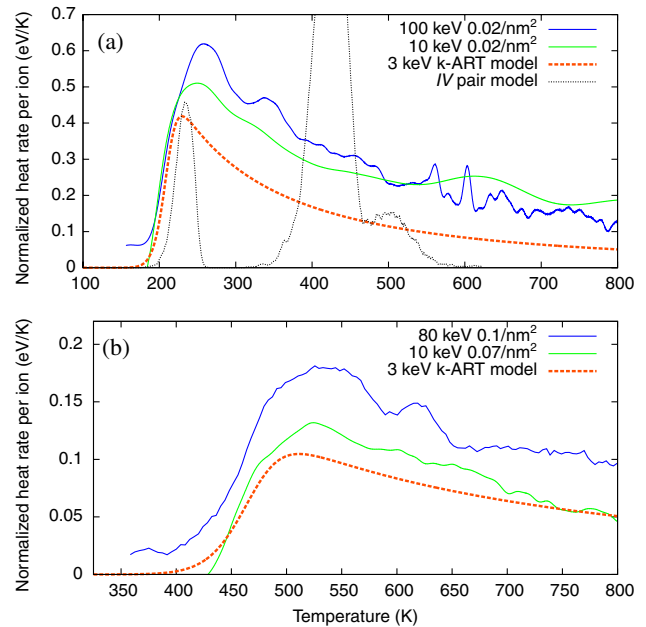


FIG. 1 (color online). Heat release as a function of temperature starting from (a) liquid nitrogen (LN) and (b) at room temperature. Solid lines: Experimental results; the NC signals are divided by the number of implanted ions and scaled to 3 keV (see text). Dashed red lines: Model derived from k-ART after 3 keV Si ion implantations. Dotted black curve: Simulation based on the *IV*-pair model at LN temperature.

We first compare experiments to the *IV*-pair model proposed by Marqués and co-workers [22,24] using as input the list of defects predicted by SRIM (stopping and range of ions in matter, an ion transport simulation code based on the central potential, binary collision, and random phase approximations) with an 80 keV implantation [19]. Defects are then evolved using lattice-based KMC annealing during and after implantation with an activation energy E_{act} that depends on the number n of nearest neighbors in the “*IV*-pair” state [24]. The simulation involves a 30 s waiting period at the lowest temperature to account for the delay between the end of the implantation and the beginning of the NC temperature scan. A typical result of our implementation of this model, with a displacement energy of 5 eV and at liquid nitrogen temperature, is presented in Fig. 1(a) (dotted curve) with the signal scaled by $3/80$ to compare to experiments and other models. The simulation shows an isolated peak at 230 K, associated with the annealing of isolated *IV* pairs ($n = 0$) associated with activation energy of 0.43 eV, followed by a series of peaks corresponding to the other activation energies ($n > 0$), and fails to reproduce experiments. Clearly, important relaxation mechanisms are missing from this lattice-based KMC model.

It could be argued that the energy released by the annealing of the *IV* pairs with different number of neighbors is not the same, especially in the case of isolated *IV* pairs, but this would only modify the amplitude of the

peaks, not their shape. Using MD [21] instead of SRIM to determine the defect's position changes the distribution of the IV pairs in the initial population, producing a higher temperature tail in the case of more concentrated damage, but the shape of the experimental signal is not reproduced.

To attempt to better capture the complex relaxation between the various structures forming the disorder, we turn to k-ART, an off-lattice self-learning KMC method. k-ART couples ART nouveau for the event search with a topological analysis tool for the catalog building and with a KMC algorithm for the time propagation [29,30]. By performing an extensive search for saddle points and fully relaxing the relevant energy barriers before each event, k-ART is able to take into account short- and long-range elastic effects. The topological analysis, performed with NAUTY [37], allows a stable and reliable management of events even for disordered and complex configurations such as vacancy diffusion in Fe [38] and relaxation in amorphous silicon [30].

We first inject a 3 keV Si atom into a 300 K 100 000-atom slab of Stillinger-Weber silicon with a Langevin bath as boundary condition perpendicular to the trajectory of the implanted atom, simulating the effect of a low-energy low-fluence ion-implantation experiment. The cell is then relaxed using MD for 1–10 ns. A 27 000-atom subpart of the cell containing the defects is then cut out and placed into a box with periodic boundary conditions along all directions, to eliminate surface effects. We generated three independent samples following this procedure and then launched several 300 K k-ART simulations on each MD-produced cascade, simulating up to time scales of 1 s or more.

Energy evolution for the k-ART trajectories is shown in Fig. 2(a). Each relaxation simulation shows a logarithmic time dependence over many orders of magnitude with a slope determined by the initial disordered configuration; independent k-ART simulations starting from the same initial model follow a similar relaxation pathway. Such logarithmic relation is similar to that observed in heat-release and relaxation experiments in other complex systems such as polymer glasses [12]. After averaging over the various simulations, in order to reproduce experimental measures over a large number of cascades, we find a slightly curved but still logarithmic overall relaxation behavior for the system that is robust to the addition or subtraction of other runs [Fig. 2(b)].

Before examining in more detail the atomistic mechanisms leading to the macroscopic relaxation, we need to confirm that the simulation results reproduce the experimental data. For this, it is necessary to convert our fixed temperature results into constant-heating energy release. We consider an initial density of processes $n(E, t = 0)$ that can be activated by first order kinetics. The number of activated events with a barrier between E and $E + dE$ during the time interval between t and $t + dt$ is

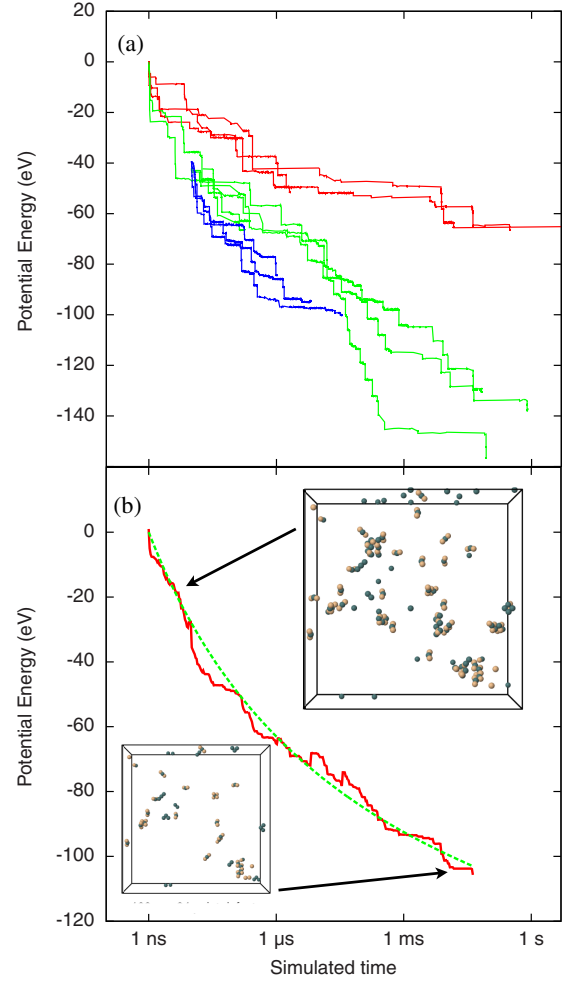


FIG. 2 (color online). (a) Energy evolution for k-ART simulations. The lines correspond to independent simulations starting from three different implantation runs. (b) Red solid line: Average of the curves in (a). Green dashed curve: Solution of Eq. (1) at $T = 300$ K. Insets: Typical configurations of defects in a 27 000-atom system after a 10 ns MD run (upper-right panel; there are 184 point defects) and after a 0.1 s k-ART simulation (lower-left panel; there are 94 point defects). Interstitials are light gray (beige) and vacancies are dark gray (blue).

$$dn(E, t)dE = -n(E, t)ve^{-E/kT}dEdt. \quad (1)$$

This equation can be solved at fixed (similar to the simulation) or increasing temperature (such as in NC scans).

Following the analysis of the accepted events, and in agreement with previous work [28], we assume that activated processes release a fixed amount of energy h_0 , independent of barrier height. A direct analysis of the microscopic events indicates that the effective $n(E, 0)$, which is kinetically determined, goes like $n(E, 0) \propto E^\mu$, with $-2.0 < \mu < -1.2$. To improve accuracy, we fit Eq. (1) to the averaged fixed temperature energy relaxation shown in Fig. 2(b) and find that the event density per interval, $\log(t)$, decreases with increasing time, in

agreement with the direct estimation, and that $h_0 n(t=0) = 53E^{-1.7}$. With this distribution, we compute the heat released under experimental conditions, including an initial annealing period of 30 s at the implantation temperature to reflect experimental conditions. Results are shown in Figs. 1(a) and 1(b). The agreement between simulation-derived energy release and experiments at both LN and RT is excellent, especially considering that the simulations are performed with an empirical potential.

The correspondence between simulations and experiments is nontrivial. A uniform density of process, $n(E, t=0)$, for example, would lead to a flat heat release such as that observed in higher implantation fluences [36] and *a*-Si [14,28]. The origin of the exponent in the density of processes is therefore associated with a decrease in the number of available barriers as defects anneal, a behavior that does not take place when amorphous pockets remain present. This decrease in complexity is observed in the microscopic evolution. After 1 ns following the implantation, before the k-ART simulation, the various models contain between 100 and 150 point defects (*I* or *V*) assembled into 20–30 clusters. Although these clusters vary in size from 1 to 30 point defects, most of them contain between 2 and 5 defects and are therefore better classified as defect complexes rather than amorphous pockets. After 1 ms to 1 s, the various simulations lead to a range of configurations that consist, typically, of small defect complexes, with 3–5 point defects, and only a few clusters. This is illustrated in the insets of Fig. 2(b), that shows typical configurations after 10 ns and 0.1 s.

Structural information is not sufficient to explain the logarithmic relaxation. Figure 3(a) shows the energy barrier separating each state selected by k-ART, aggregated over the simulations that reached at least $10 \mu\text{s}$, as a function of time. Two features stand out. First, a quasicontinuous distribution of activated events is accessible in all time frames. Even after relaxing the system by several tens of eV, low-barrier events are still present and executed. Second, the maximum energy barrier for executed events increases logarithmically with time.

The quasicontinuous barrier distribution suggests that the system can be kinetically limited by configurational entropy. Most of the low-energy barriers connect flickering states that do not lead to structural evolution. The logarithmically growing maximum energy barriers, for their part, indicate that the structural evolution is also energy limited and it is this interplay that generates a logarithmic energy decay.

The link between energy relaxation and kinetics is given by the high-energy barriers. The inset of Fig. 3(a) shows the heat released by the events with an energy barrier above the 90th percentile, i.e., those above the straight line. These do not generally lead to large drops in potential energy and many even lead to a higher-energy state, in agreement with recent observations that the forward and

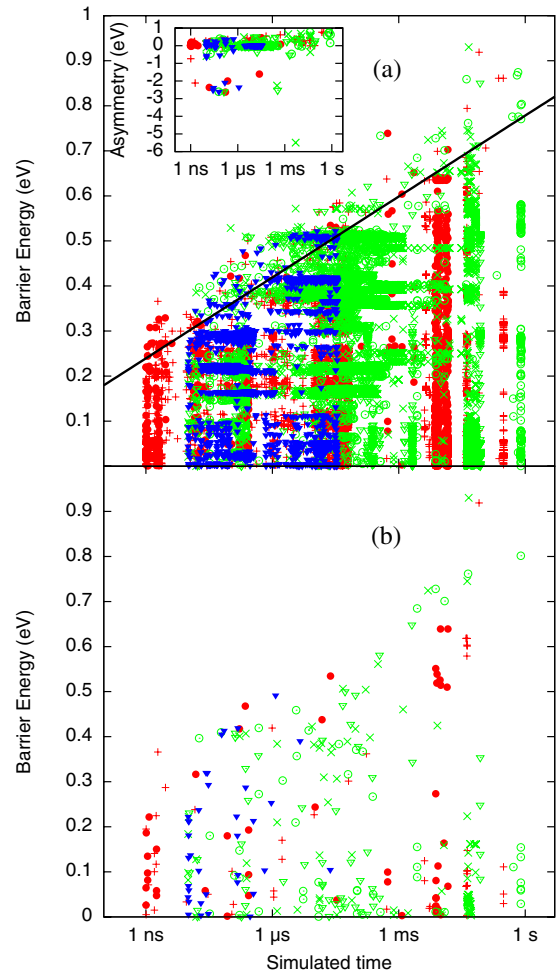


FIG. 3 (color online). (a) Energy barrier of all executed k-ART events. Points above the solid black line correspond to the 10% highest energy barriers in each time frame. Inset: Potential energy asymmetry (final energy minus initial energy) of the executed events with an energy barrier lying in the top 10% of the barriers plotted in (a) for each time frame. (b) Energy barrier of the k-ART events that release at least 0.5 eV of heat.

reverse energy barriers are totally uncorrelated [28]; the energy barrier of events that lead directly to a significant relaxation are distributed evenly throughout all the selected events [Fig. 3(b)]. Our simulations indicate that the annealing of the implanted *c*-Si is not systematically kinetically limited by the relaxation events, but is limited by events that allow the system to leave a region of the configurational space where the potential energy landscape is essentially flat to reach another region where a large drop in potential energy is accessible. It can be described as a two-step replenish and relax process that explains the logarithmic relaxation. High-energy barrier events, which are mostly reconfiguration events, do not directly lead to a low-energy structure but rather unlock the system, open new low-energy pathways, and replenish the basin of available energy-releasing events. These events are associated with an almost continuous and time-independent

energy barrier distribution that reflects the complexity of the defects themselves and the impact of long-range elastic deformations.

The authors are grateful to S. Roorda for fruitful discussion, L. Godbout, X. Perraton, and R. Gosselin for their excellent technical assistance, M. Skvarla and P. Infante of the Cornell Nanofabrication Facility, as well as M. H. Bernier and P. Vasseur of École Polytechnique de Montréal for their assistance with NC fabrication. We thank Calcul Québec for generous allocation of computer resources. This work benefited from the financial support of NanoQuébec, the Fonds québécois de recherche sur la nature et les technologies, the Natural Science and Engineering Research Council of Canada, and the Canada Research Chair Foundation. The k-ART software package can be obtained via N. M.

*laurent.karim.beland@umontreal.ca

†y.anahory@gmail.com

‡Current address: Department of Physics and Centre for Scientific Computing, University of Warwick, Gibbet Hill Road, Coventry CV4 7AL, United Kingdom.

p.brommer@warwick.ac.uk

§jeanf.joly@gmail.com

||jc.pothier@phytronix.com

¶laurent.lewis@umontreal.ca

**normand.mousseau@umontreal.ca

††francois.schiettekatte@umontreal.ca

- [1] D. J. Plazek, K. L. Ngai, and R. W. Rendell, *Polym. Eng. Sci.* **24**, 1111 (1984).
- [2] P. K. Dixon, L. Wu, S. R. Nagel, B. D. Williams, and J. P. Carini, *Phys. Rev. Lett.* **65**, 1108 (1990).
- [3] J. P. Sethna, J. D. Shore, and M. Huang, *Phys. Rev. B* **44**, 4943 (1991).
- [4] R. Böhmer, K. Ngai, C. Angell, and D. Plazek, *J. Chem. Phys.* **99**, 4201 (1993).
- [5] L. F. Cugliandolo and J. Kurchan, *Phys. Rev. Lett.* **71**, 173 (1993).
- [6] E. Vincent, J. P. Bouchaud, D. S. Dean, and J. Hammann, *Phys. Rev. B* **52**, 1050 (1995).
- [7] L. Andreozzi, M. Faetti, M. Giordano, and D. Palazzuoli, *J. Phys. Condens. Matter* **15**, S1215 (2003).
- [8] K. Chen and K. S. Schweizer, *Phys. Rev. Lett.* **98**, 167802 (2007).
- [9] J. C. Phillips, *Rep. Prog. Phys.* **59**, 1133 (1996).
- [10] A. Amir, Y. Oreg, and Y. Imry, *Proc. Natl. Acad. Sci. U.S.A.* **109**, 1850 (2012).
- [11] G. B. McKenna, *J. Phys. Condens. Matter* **15**, S737 (2003).
- [12] A. Knoll, D. Wiesmann, B. Gotsmann, and U. Duerig, *Phys. Rev. Lett.* **102**, 117801 (2009).
- [13] A. Sepúlveda, E. Leon-Gutierrez, M. Gonzalez-Silveira, C. Rodríguez-Tinoco, M. T. Clavaguera-Mora, and J. Rodríguez-Viejo, *Phys. Rev. Lett.* **107**, 025901 (2011).
- [14] J. F. Mercure, R. Karmouch, Y. Anahory, S. Roorda, and F. Schiettekatte, *Phys. Rev. B* **71**, 134205 (2005).
- [15] P. Roura and J. Farjas, *Acta Mater.* **57**, 2098 (2009).
- [16] P. Roura and J. Farjas, *Phys. Rev. Lett.* **103**, 119801 (2009).
- [17] M. J. Caturla, T. Díaz de la Rubia, L. A. Marqués, and G. H. Gilmer, *Phys. Rev. B* **54**, 16683 (1996).
- [18] M. J. Beck, R. D. Schrimpf, D. M. Fleetwood, and S. T. Pantelides, *Phys. Rev. Lett.* **100**, 185502 (2008).
- [19] J. Ziegler, J. Biersack, and U. Littmark, *The Stopping and Range of Ions in Matter* (Pergamon, New York, 1985), 1st ed.
- [20] K. Nordlund, M. Ghaly, R. S. Averback, M. Caturla, T. Diaz de la Rubia, and J. Tarus, *Phys. Rev. B* **57**, 7556 (1998).
- [21] J.-C. Pothier, F. Schiettekatte, and L. J. Lewis, *Phys. Rev. B* **83**, 235206 (2011).
- [22] L. Pelaz, L. A. Marqués, and J. Barbolla, *J. Appl. Phys.* **96**, 5947 (2004).
- [23] S. Donnelly, R. Birtcher, V. Vishnyakov, and G. Carter, *Appl. Phys. Lett.* **82**, 1860 (2003).
- [24] L. A. Marqués, L. Pelaz, M. Aboy, L. Enríquez, and J. Barbolla, *Phys. Rev. Lett.* **91**, 135504 (2003).
- [25] F. Wooten, K. Winer, and D. Weaire, *Phys. Rev. Lett.* **54**, 1392 (1985).
- [26] D. M. Stock, B. Weber, and K. Gärtner, *Phys. Rev. B* **61**, 8150 (2000).
- [27] F. Valiquette and N. Mousseau, *Phys. Rev. B* **68**, 125209 (2003).
- [28] H. Kallel, N. Mousseau, and F. Schiettekatte, *Phys. Rev. Lett.* **105**, 045503 (2010).
- [29] F. El-Mellouhi, N. Mousseau, and L. J. Lewis, *Phys. Rev. B* **78**, 153202 (2008).
- [30] L. K. Béland, P. Brommer, F. El-Mellouhi, J.-F. Joly, and N. Mousseau, *Phys. Rev. E* **84**, 046704 (2011).
- [31] M. Efremov, E. Olson, M. Zhang, F. Schiettekatte, Z. Zhang, and L. Allen, *Rev. Sci. Instrum.* **75**, 179 (2004).
- [32] R. Karmouch, J.-F. Mercure, and F. Schiettekatte, *Thermochim. Acta* **432**, 186 (2005).
- [33] M. Y. Efremov, F. Schiettekatte, M. Zhang, E. A. Olson, A. T. Kwan, R. S. Berry, and L. H. Allen, *Phys. Rev. Lett.* **85**, 3560 (2000).
- [34] R. Karmouch, Y. Anahory, J.-F. Mercure, D. Bouilly, M. Chicoine, G. Bentoumi, R. Leonelli, Y. Q. Wang, and F. Schiettekatte, *Phys. Rev. B* **75**, 075304 (2007).
- [35] Y. Anahory, M. Guihard, D. Smeets, R. Karmouch, F. Schiettekatte, P. Vasseur, P. Desjardins, L. Hu, L. Allen, E. Leon-Gutierrez, and J. Rodriguez-Viejo, *Thermochim. Acta* **510**, 126 (2010).
- [36] Y. Anahory, Ph.D. thesis, Université de Montréal, 2011, https://papyrus.bib.umontreal.ca/xmlui/bitstream/handle/1866/4657/Anahory_Yonathan_2010_these.pdf.
- [37] B. D. McKay, *Congr. Numer.* **30**, 45 (1981), <http://cs.anu.edu.au/~bdm/nauty/pgi.pdf>.
- [38] P. Brommer and N. Mousseau, *Phys. Rev. Lett.* **108**, 219601 (2012).